processes

MDPI

Article

Optimization of a Tricalcium Phosphate-Based Bone Model Using Cell-Sheet Technology to Simulate Bone Disorders

Alexandra Damerau [1,2], Frank Buttgereit [1,2] and Timo Gaber [1,2,*]

[1] Department of Rheumatology and Clinical Immunology, Charité-Universitätsmedizin Berlin, Corporate Member of Freie Universität Berlin, Humboldt-Universität zu Berlin, 10117 Berlin, Germany; alexandra.damerau@charite.de (A.D.); frank.buttgereit@charite.de (F.B.)
[2] Deutsches Rheuma-Forschungszentrum (DRFZ), Institute of the Leibniz Association, 10117 Berlin, Germany
* Correspondence: timo.gaber@charite.de

Abstract: Bone diseases such as osteoporosis, delayed or impaired bone healing, and osteoarthritis still represent a social, financial, and personal burden for affected patients and society. Fully humanized in vitro 3D models of cancellous bone tissue are needed to develop new treatment strategies and meet patient-specific needs. Here, we demonstrate a successful cell-sheet-based process for optimized mesenchymal stromal cell (MSC) seeding on a β-tricalcium phosphate (TCP) scaffold to generate 3D models of cancellous bone tissue. Therefore, we seeded MSCs onto the β-TCP scaffold, induced osteogenic differentiation, and wrapped a single osteogenically induced MSC sheet around the pre-seeded scaffold. Comparing the wrapped with an unwrapped scaffold, we did not detect any differences in cell viability and structural integrity but a higher cell seeding rate with osteoid-like granular structures, an indicator of enhanced calcification. Finally, gene expression analysis showed a reduction in chondrogenic and adipogenic markers, but an increase in osteogenic markers in MSCs seeded on wrapped scaffolds. We conclude from these data that additional wrapping of pre-seeded scaffolds will provide a local niche that enhances osteogenic differentiation while repressing chondrogenic and adipogenic differentiation. This approach will eventually lead to optimized preclinical in vitro 3D models of cancellous bone tissue to develop new treatment strategies.

Keywords: mesenchymal stromal cell; cell sheet; osteogenesis; β-TCP; tricalcium phosphate; tissue engineering; in vitro 3D model

Citation: Damerau, A.; Buttgereit, F.; Gaber, T. Optimization of a Tricalcium Phosphate-Based Bone Model Using Cell-Sheet Technology to Simulate Bone Disorders. *Processes* **2022**, *10*, 550. https://doi.org/10.3390/pr10030550

Academic Editor: Clayton Jeffryes

Received: 4 February 2022
Accepted: 7 March 2022
Published: 11 March 2022

1. Introduction

Bone defects and healing disorders arise from various causes such as fractures, other traumas, tumors, infections, dental restorations, healing disorders, and congenital malformations. They can lead to pain and significant loss of quality of life [1–3]. The prevalence of bone diseases and healing disorders increases with life expectancy [4,5]. Both regenerating bone defects and treating healing disorders represent considerable challenges for clinicians. Autologous grafts from the iliac crest remain the gold standard; even though their availability is limited, they carry a risk of infection, and there is only little autologous bone material available [6,7]. Over the past two decades, significant progress has been achieved in developing tissue engineering concepts for the production of synthetic bone substitutes that overcome these challenges by adding new possibilities to standard surgical procedures for the treatment of these patients [2,3].

Clinically, tissue-engineered bone restoration relies on the generation of neo-tissues from osteogenic progenitor cells alone or with the support of osteoconductive bone substitutes for bone ingrowth and osteoinductive growth factors, with and without the need of supportive metal implants [2,3,8]. Although preclinical data from animal studies are often promising, the clinical failure of implants, bone substitutes, and osteoinductive agents is apparent because of limited animal-to-human predictability due to differences in, for

example, physiology, genetics, epigenetics, and molecular biology between species [9,10]. This is also a problem when dealing with bone substitutes coated with osteoinductive growth factors that work in animal models but fail in humans.

Preclinically, tissue-engineered in vitro 3D bone models can improve our understanding of bone biology's physiological and pathophysiological mechanisms (e.g., avascular osteonecrosis). These models may also serve as predictive models of implant success or failure concerning osteoconductive properties of novel biomaterials for bone regeneration. In addition, in vitro 3D bone models provide the opportunity to test, verify, and evaluate novel osteoinductive substances or other therapeutical attempts (e.g., anti-osteoporotic drugs) in a human-based laboratory setting or may directly be used as a clinical implant [11]. However, due to the lack of sophisticated in vitro 3D models, animal models still remain the gold standard, even though great differences in (patho) physiology led to low transferability [12,13].

To simulate native bone in vitro, various tissue engineering approaches have been pursued, including scaffold-based, scaffold-free, and more sophisticated microfluidic model systems that implement a variety of cell or tissue types [14,15]. The most common in vitro 3D approach involves seeding osteogenic progenitor cells on synthetic bone graft substitutes that mimic the mineral bone part, followed by static cultivation, perfused cultivation, or dynamic mechanical loading during cultivation. Artificial bone graft substitutes differ in biocompatibility, immunogenicity, biological activity, cell–biomaterial interactions, and mechanical properties [16]. Additional limitations include low cell attachment efficiency and heterogeneous cellular distribution [17]. Calcium phosphate-based bioceramics that mimic the inorganic bone component have been extensively studied for their applicability. The most common bioceramics are β-tricalcium phosphate (β-TCP), hydroxyapatite (HA), and a mixture of the two known as biphasic calcium phosphate (BCP)-HA/β-TCP—which are well researched and have been reported to support cell adhesion, tissue formation, and differentiation [18–20].

Conventional approaches usually focus on the injection of isolated cell suspensions or the use of pre-seeded biodegradable scaffolds to support tissue formation, depriving cells of their endogenous extracellular matrix (ECM). However, it is challenging to ensure reproducible cell-seeding efficiency [21,22]. In addition, scaffold-based and scaffold-free models are often produced on a small scale with few scaffold particles or cell spheroids. Thus, optimized cell seeding and up-sizing without altering manufacturing conditions are significant challenges in the fabrication of complex in vitro models. Moreover, in the clinical situation, the microenvironment of the bone and surrounding cells are involved in the regeneration process [7]. These conditions are missing and need to be mimicked in developing preclinical models, enhancing translational and clinical success [2,3].

The cell-sheet technology offers the possibility to compensate for these deficits in conventional approaches. This technology enables the generation of viable, transplantable cell sheets from monolayer cell cultures, e.g., using temperature-dependent plates [17,22]. These plates allow cells to be harvested while preserving cell–cell junctions and the ECM without using proteolytic enzymes, allowing for cell-dense tissues [22–25]. Cell-sheet technology has already been successfully used for proper tissue regeneration in periosteum [26], corneal epithelial, myocardial, and—of note—in bone tissues [24,27–29]. However, the development of grafts for bone regeneration is still in its infancy. The difficulty is replicating the high level of bone hierarchical organization while considering the anabolic and catabolic processes.

In bone regeneration, adult mesenchymal stromal cells (MSCs)—the progenitor cells of the anabolic bone compartment—are well suited for the cell-sheet technology approach. MSCs are "self-renewable, multipotent, easily accessible and culturally expandable in vitro with exceptional genomic stability and few ethical issues, marking its importance in cell therapy, regenerative medicine and tissue repairment" [30]. Moreover, MSCs own the potential to modulate and suppress immune responses and thus reduce graft rejection or graft-versus-host reactions [31–33]. Therefore, MSC-based cell-sheets have attracted increasing attention

as a tool to accelerate bone healing, treat chronic pain and infection, and minimize immunological reactions associated with allogeneic bone graft substitutes [24,34]. Interestingly, thin MSC-based cell-sheets can spontaneously form vascular or pre-vascularized capillaries with endothelial (progenitor) cells to facilitate vascularization and integration into the host anatomy [35,36]. Finally, the envelopment of osteoclasts and osteoblasts/osteocytes and immune cells in the MSC-based cell sheets in vitro allows mapping both catabolic and anabolic processes and immunological processes in the bone marrow.

In a previous study, we used a scaffold-based model and seeded MSCs on the biodegradable β-TCP scaffold to mimic cancellous bone [37]. We could demonstrate that these MSCs showed osteogenic properties in vitro, evidenced by the high expression of collagen type 1 (*COL1A1*), osteocalcin (*OC*), osteonectin (*ON*), and bone formation via µCT analysis. However, we observed that porous scaffolds, such as β-TCP, are hardly populated by cells. Given this background, we evaluated osteogenically induced MSC-based cell sheets wrapped around a human in vitro 3D bone model comprising a pre-seeded β-TCP scaffold for cell seeding and differentiation efficiency.

To evaluate our human sheet-based in vitro 3D bone model, we analyzed its response to osteoinductive deferoxamine (DFO). Several studies have already demonstrated the efficacy of DFO in promoting bone fracture healing in a variety of animal models (mouse, rat, and rabbit) with different bone defects (calvaria defect or critical size defect) [38–51]. DFO treatment promotes angiogenesis/vessel formation and bone regeneration independent of the species, model, and evaluation methods [39–57]. Using well-characterized MSCs, we previously demonstrated that HIF-1 promotes osteogenesis and suppresses adipogenesis by loss of function experiments and by pharmacological intervention using DFO [58]. Therefore, we investigated the applicability and response to DFO in this human MSC-sheet-based in vitro 3D bone model, ultimately serving as a human-based preclinical model providing transferability and reducing the number of animal experiments.

2. Materials and Methods

2.1. Bone Marrow-Derived MSC Isolation and Cultivation

Human bone marrow was provided by the Center of Musculoskeletal Surgery, Charité-Universitätsmedizin Berlin, and obtained from patients undergoing total hip replacement (Table 1). Protocols and study design were performed according to the Helsinki Declaration and approved by the Charité-Universitätsmedizin Ethics Committee (ethical approval EA1/146/21; EA1/012/13).

Table 1. Data on age and sex of human MSCs used.

Donor	Age	Sex	Donor	Age	Sex
1	56	male	6	62	female
2	69	female	7	77	male
3	71	male	8	64	female
4	81	female	9	65	male
5	75	female	10	58	male

For isolation of MSCs, bone marrow was placed in a T-175 flask (Greiner Bio-one International GmbH, Kremsmünster, Austria). MSCs—ability to adhere to plastic—were cultured in Dulbecco's Modified eagle Minimal Essential Medium with GlutaMAX™ (DMEM, Gibco, Waltham, MA, USA) supplemented with 10% fetal calf serum (FCS, Biowest, Nuaillé, France), 100 U/mL penicillin (Gibco), 100 µg/mL streptomycin (Gibco, Waltham, MA, USA), and 20% StemMACS™ MSC Expansion Media Kit XF (Miltenyi Biotech, Bergisch Gladbach, Germany). The remaining bone marrow tissue parts were removed after 48 h. The medium was changed weekly, and passaging was performed when reaching 85–90% confluence. Cells were used until passage 6. MSC characterization was performed as described previously in detail [37,59].

2.2. Fabrication of 3D Bone Models: β-TCP Wrapped with an Osteogenically Induced MSC Sheet

To mimic the mineral part of cancellous bone most closely, we used clinical-grade, biocompatible and resorbable β-TCP (Cerasorb®M, Curasan AG, Kleinostheim, Germany) with a particle size range from 1000 to 2000 µm, which provides an interconnecting, open multiporosity with micro-, meso- and macropores (5–500 µm) and total porosity of approximately 65%. Notably, particles of this size most closely mimicked the properties of cancellous bone about bone formation trabecular numbers and thickness in a model of bone formation, whereas the chemical composition had only a minor influence [60].

We preincubated 12 mg of β-TCP with DMEM GlutaMAX™ supplemented with 10% FCS, 100 U/mL penicillin, and 100 µg/mL streptomycin for 24 h. Subsequently, we pre-seeded β-TCP with a suspension of 1×10^6 MSCs and cultured them in tissue culture inserts in a 24-well plate (Sarstedt, Nümbrecht, Germany) to ensure adequate nutrient supply (in the following abbreviated as 'TCP'). Osteogenic differentiation was induced using DMEM supplemented with 10% FCS, 100 U/mL penicillin, 100 µg/mL streptomycin, 0.5 mM ascorbic acid, 10^{-8} M dexamethasone, and 10 mM L-glycerophosphate (osteogenic medium). A single osteogenically induced MSC sheet was developed by culturing 1×10^6 cells in a 35 mm temperature-responsive dish (Nunc™, Merck, Darmstadt, Germany) with an osteogenic medium for 7 days. On day 7, the single cell-sheet was harvested by decreasing the temperature under 32 °C and then wrapped around the pre-seeded β-TCP scaffold (cell-sheet-based β-TCP, in the following abbreviated as 'csTCP'). In total, the TCP and csTCP model was osteogenically differentiated for 21 days.

2.3. Live/Dead Staining

To visualize the colonization of viable cells in 3D, LIVE/DEAD® Viability/Cytotoxicity Kit (Invitrogen AG, Carlsbad, CA, USA) was performed: After a washing step with 1 × PBS, the staining solution consisting of 2 µM Calcein-AM and 4 µM EthD-1 was added to the 3D models and incubated for 35 min at room temperature in the dark. Imaging was performed using the fluorescence microscope BZ-9000 (Keyence, Neu-Isenburg, Germany).

2.4. TUNEL Assay

Detecting apoptotic cells, TUNEL staining (Sigma-Aldrich, Munich, Germany) was performed with 5 µL TUNEL enzyme and 45 µL TUNEL label for one hour at 37 °C. After washing with 1 × PBS (twice), images were acquired using a BZ-9000 fluorescence microscope (Keyence). Slices treated with deoxyribonuclease (DNase) I (0.34 Kunitz units, Qiagen, Hilden, Germany) for 10 min were positive, while the negative control was incubated without the TUNEL enzyme.

2.5. Scanning Electron Microscopy (SEM)

Using SEM, scaffolds seeded with cells with and without an additional MSC sheet were examined for cellular colonialization, distribution, and cell morphology. After a washing step with 1 × PBS, samples were fixed with 2.5% glutaraldehyde (Sigma-Aldrich) for 10 min and then washed again. Afterward, samples were stepwise dewatered in an ascending ethanol order—30%, 50%, 70%, 80%, 90%, 95%, and twice 100%—for 5 min each, followed by hexamethyldisilazane (1 × 5 min, 2 × 10 min; Sigma-Aldrich). Finally, all samples were dried overnight. After gold coating using the Fine Coater JFC 1200 (Jeol GmbH, Freising, Germany), images were acquired using the scanning electron microscope JCM-6000 Plus Neo Scope™ (Jeol GmbH).

2.6. (Immun)Histochemistry

Kawamoto cryofilm type 2C (Sectionlab, Hiroshima, Japan) was used to prepare 7 µm cryo-sections. Slices were air-dried before each staining protocol, then fixed in 4% paraformaldehyde (PFA, Electron Microscopy Sciences, Hatfield, PA, USA), and subsequently washed with ddH_2O. After every staining protocol, cryo-sections were covered with DPX Mountant (Sigma-Aldrich).

Hematoxylin and Eosin (H & E) staining was performed using Harris's hematoxylin (Merck, Darmstadt, Germany) for 7 min, then washed with ddH_2O, followed by a differentiation step with 0.25% HCl–ethanol (Merck). Eosin staining (0.2%, 2 min; Chroma Waldeck GmbH & Co. KG, Münster, Germany) was performed after 10 min in tap water, followed by 96% ethanol, 100% ethanol, and xylol (2 min, twice).

Collagen type I staining was performed as follows: 3% H_2O_2 for 30 min, washing step with 1 × PBS for 5 min. After a blocking step with 1 × PBS/5% normal horse serum (HS, Vector Laboratories, Burlingame, CA, USA)/2% bovine serum albumin (BSA, Sigma-Aldrich), staining with anti-collagen type I (1:500, Abcam, Cambridge, UK) was performed overnight at 4 °C. Slices were washed with 1 × PBS, followed by an incubation step with 2% biotinylated horse anti-mouse IgG antibody (Vector Laboratories; diluted in 1 × PBS/5% HS/2% BSA) at room temperature for 30 min. After a washing step, slices were incubated with Vecastain® Elite® ABC HRP Kit (Vector Laboratories) for 50 min, washed with 1 × PBS, and set with DAB Peroxidase HRP Substrate Kit (Vector Laboratories). Finally, counterstaining was performed with Mayer's hematoxylin (2 min, Sigma-Aldrich).

2.7. Immunofluorescence Staining

For the immunofluorescence staining, slices were rehydrated with 1 × PBS for 10 min and permeabilized with 0.1% Tween 20® (Sigma-Aldrich) in 1 × PBS for 20 min. After a blocking step with 5% FCS in 1 × PBS for 30 min, cells were washed three times with 1 × PBS/0.1% Tween 20® and incubated with phalloidin-TRITC (Sigma-Aldrich; working solution: 10 µg/mL in 1 × PBS/0.1% Tween 20®/5% FCS) for 45 min or the primary osteopontin antibody (Abcam; 1:50 in 1 × PBS/5% FCS/0.1% Tween 20®) for 2 h. After a washing step, the secondary donkey anti-goat A568 antibody (Thermo Fisher Scientific, Waltham, MA, USA; 1:500 in 1 × PBS/5% FCS/0.1% Tween 20®) was applied for 1 h. Finally, after washing with 1 × PBS/0.1% Tween 20®, the visualization of nuclear DNA was performed using 1 µg/mL 4′,6-diamidino-2-phenylindo (DAPI; Life Technologies, Carlsbad, CA, USA; diluted in 1 × PBS/0.1% Tween 20®/5% FCS) for 15 min. Cryosections were covered with Fluoromount™ (Sigma-Aldrich). Images were performed using a fluorescence microscope (BZ-9000; Keyence).

2.8. Gene Expression Analysis

TCPs were transferred to 300 µL RLT-buffer (Qiagen) with 1% 2-mercaptoethanol (Serva Electrophoresis GmbH, Heidelberg, Germany) and homogenized using the TissueRuptor II (Qiagen). According to the manufacturer's instructions, total RNA was isolated using the RNeasy® Fibrous Tissue Mini Kit (Qiagen). Nanodrop ND-1000 (Peqlab Biotechnologie GmbH, Erlangen, Germany) was used to determine the RNA concentration. cDNA synthesis was performed using TaqMan® Reverse Transcription Reagents Kit (Applied Biosystems Inc., Waltham, MA, USA). The DyNAmo ColorFlash SYBR Green qPCR Kit (Thermo Fisher Scientific) and the Stratagene Mx3000P™ (Agilent Technologies Inc., Santa Clara, CA, USA) were used to perform qPCR. Gene expression analysis was performed in duplicate with a non-template control for each master mix using the following temperature profile: initial denaturation for 7 min at 95 °C, denaturation for 60 cycles of 10 s at 95 °C, annealing for 7 s at 60 °C, and elongation for 9 s at 72 °C. All primers (Table 2) were purchased from TIB Molbiol and verified by sequence analysis performed by LGC Genomics.

Table 2. Sequences of primers used for qPCR.

Gene	Sequence of Forward Primer	Sequence of Reverse Primer
EF1A	GTTGATATGGTTCCTGGCAAGC	TTGCCAGCTCCAGCAGCCT
RUNX2	TTACTTACACCCCGCCAGTC	TATGGAGTGCTGCTGGTCTG
SPP1	GCCGAGGTGATAGTGTGGTT	TGAGGTGATGTCCTCGTCTG
COL1A1	CAGCCGCTTCACCTACAGC	TTTTGTATTCAATCACTGTCTTGCC
ON	ACCAGCACCCCATTGACG	AGGTCACAGGTCTCGAAAAAGC
SOX9	CGCCTTGAAGATGGCGTTG	GCTCTGGAGACTTCTGAACGA
PPARγ2	CAAACCCCTATTCCATGCTGTT	AATGGCATCTCTGTGTCAACC
IL6	TACCCCCAGGAGAAGATTCC	TTTTCTGCCAGTGCCTCTTT
IL8	GAATGGGTTTGCTAGAATGTGATA	CAGACTAGGGTTGCCAGATTTAAC
LDHA	ACCCAGTTTCCACCATGATT	CCCAAAATGCAAGGAACACT
VEGFA	AGCCTTGCCTTGCTGCTCTA	GTGCTGGCCTTGGTGAGG
PGK1	ATGGATGAGGTGGTGAAAGC	CAGTGCTCACATGGCTGACT

2.9. Statistical Analysis

Statistical analyses were performed using the software GraphPad® Prism Version 9.3.0 (La Jolla, San Diego, CA, USA). Data are shown as box plots with all data points (centerline, median; box limits, upper and lower quartiles; whiskers, maximum and minimum). For independent datasets, the Mann–Whitney U test was applied. Concerning the deferoxamine study, differences between the groups were determined with the two-tailed Wilcoxon matched-pairs signed-rank test. p-values of <0.05 were considered to be statistically significant.

3. Results

3.1. MSC-Based Cell-Sheet Wrapping Enhanced Survival Rate of MSCs Seeded on β-TCP

Since it is essential to achieve flexibility in the size of the preclinical in vitro bone model to allow for high throughput, use in a perfused cell culture chamber, or regeneration of different sized bone defects, we investigated the FDA-approved synthetic β-TCP-based bone graft substitute (1–2 mm particle size). We previously determined an optimal cell source of 0.8×10^5 cells/mg and readout parameters, such as SEM, RT-qPCR, and histology after 21 days of differentiation [37].

To enhance the handling, reproducibility, and quality of β-TCP-based cancellous bone models, we used a technique known as cell-sheet technology. We used bone-marrow-derived MSCs obtained from patients undergoing surgery for total hip replacement as a cell source. MSCs were seeded at a high density onto a temperature-responsive cell culture surface and in parallel on biodegradable β-TCP scaffolds (Figure 1A). The cell-sheet reached confluence within 2 or 3 days and formed a thin cellular sheet at 7 days. To investigate the survival of differentiated MSCs in 3D, LIVE/DEAD® and TUNEL staining was performed on day 21. Results indicated a higher survival rate—relative area of living (Calcein-AM+) cells—of osteogenically induced MSCs populated on β-TCP wrapped with a single MSC-sheet (csTCP) to the unwrapped MSC-populated β-TCP (TCP; Figure 1B,C). Taken together, combining cell-sheet technology with conventional β-TCP leads to improved survival without causing apoptosis.

3.2. CsTCPs Exhibit Higher MSC Seeding Density than Unwrapped Pre-Seeded TCPs

Next, we investigated cell adhesion to the β-TCP scaffold, morphological differences, and ECM development between the MSC-populated TCPs and csTCPs using SEM. MSCs adhered and spread on the surface of the scaffold by forming a cell layer covering the pores of the scaffold. SEM images qualitatively but reproducibly highlight that MSCs entirely colonized the biodegradable β-TCP scaffold when an additional cell sheet was used, as indicated by more significant amounts of ECM on the scaffold (Figure 2A, asterisk). Scanning the scaffold surface at specific locations and higher magnifications revealed the presence of a microstructure deposit exhibiting a unique spherical morphology. After three weeks of differentiation, the morphology of these deposits was similar to the typical calcium phosphate microstructures, demonstrating osteogenic differentiation as reported previously [61]. The proportion of cells covered with spherical deposits showed osteogenic

differentiation in both approaches, although osteogenesis appears to be more pronounced in csTCPs (Figure 2A, arrow). Furthermore, fluorescence analysis of the actin filaments confirmed a high cell density within the β-TCP particles, which was considerably higher when using the cell-sheet technology (Figure 2B). The histological evaluation of the in vitro bone model was consistent with the results of the SEM examination and immunofluorescence analysis, demonstrating a high cell density, uniform cell distribution (Figure 3A), and the presence of more significant amounts of ECM, especially in the csTCP models (Figure 3B). In summary, using cell-sheet technology, isolated MSCs attached and differentiated on and in the β-TCP scaffold.

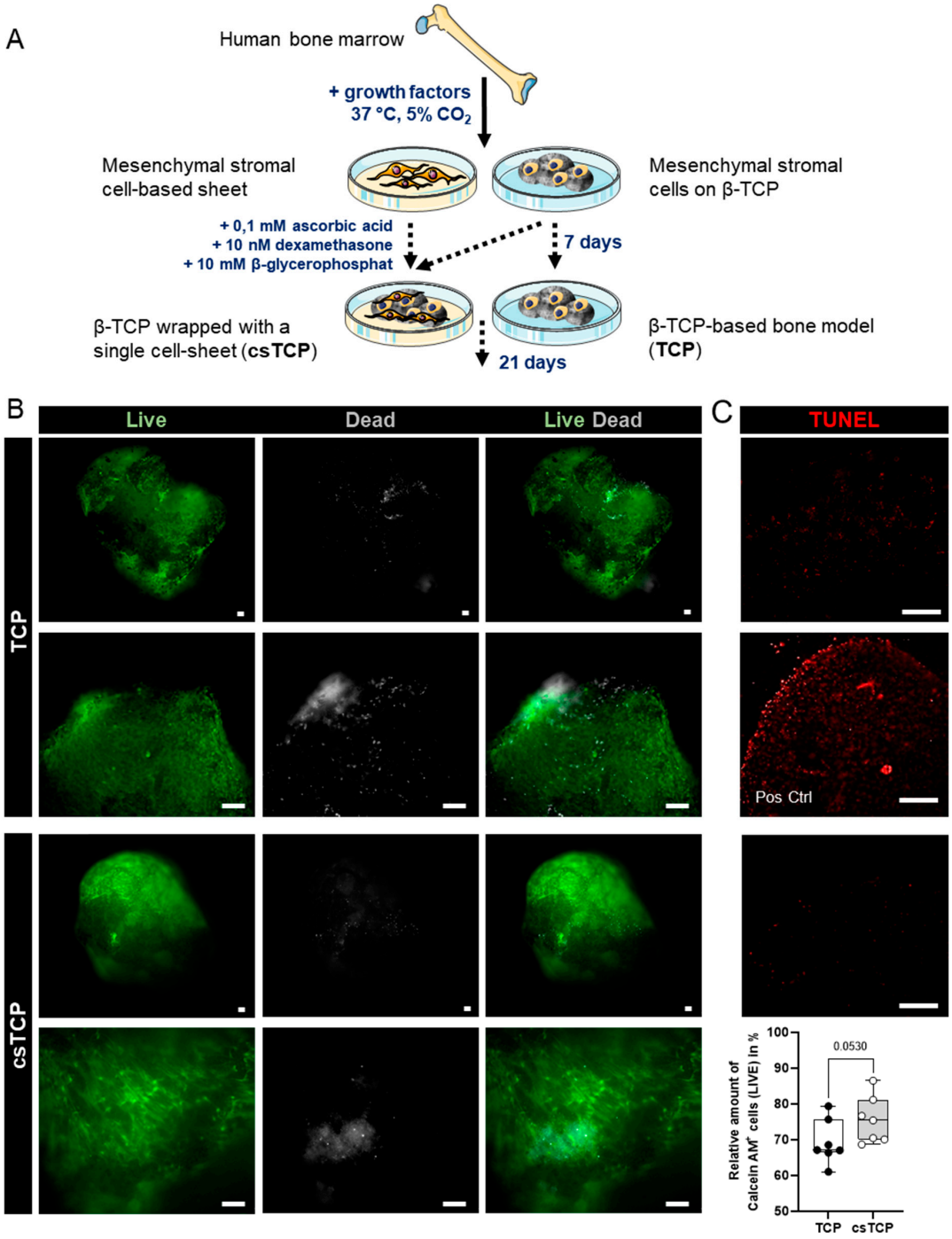

Figure 1. MSC-based cell-sheet wrapping enhanced the survival rate of MSCs seeded on TCP. (**A**) MSCs were seeded on (i) β-TCP particles (TCP) and (ii) temperature-responsive dishes. The latter

was osteogenically differentiated for 7 days, then wrapped around TCP (csTCP), and differentiated for 21 days. (**B**) Representative images of LIVE/DEAD staining were conducted at 21 days and quantified using ImageJ. Living cells are presented in green (Calcein-AM+) and dead cells in grey (EthD+). (**C**) Detection of apoptotic cells (red) using TUNEL staining at day 21 with and without cell-sheet technology. Pos Ctrl = DNase I treatment for 10 min. Data are shown as box plots (centerline, median; box limits, upper and lower quartiles; whiskers, maximum and minimum values; all data points); n = 7. Scale bars show 100 µm. Statistics: Two-tailed Mann–Whitney U test.

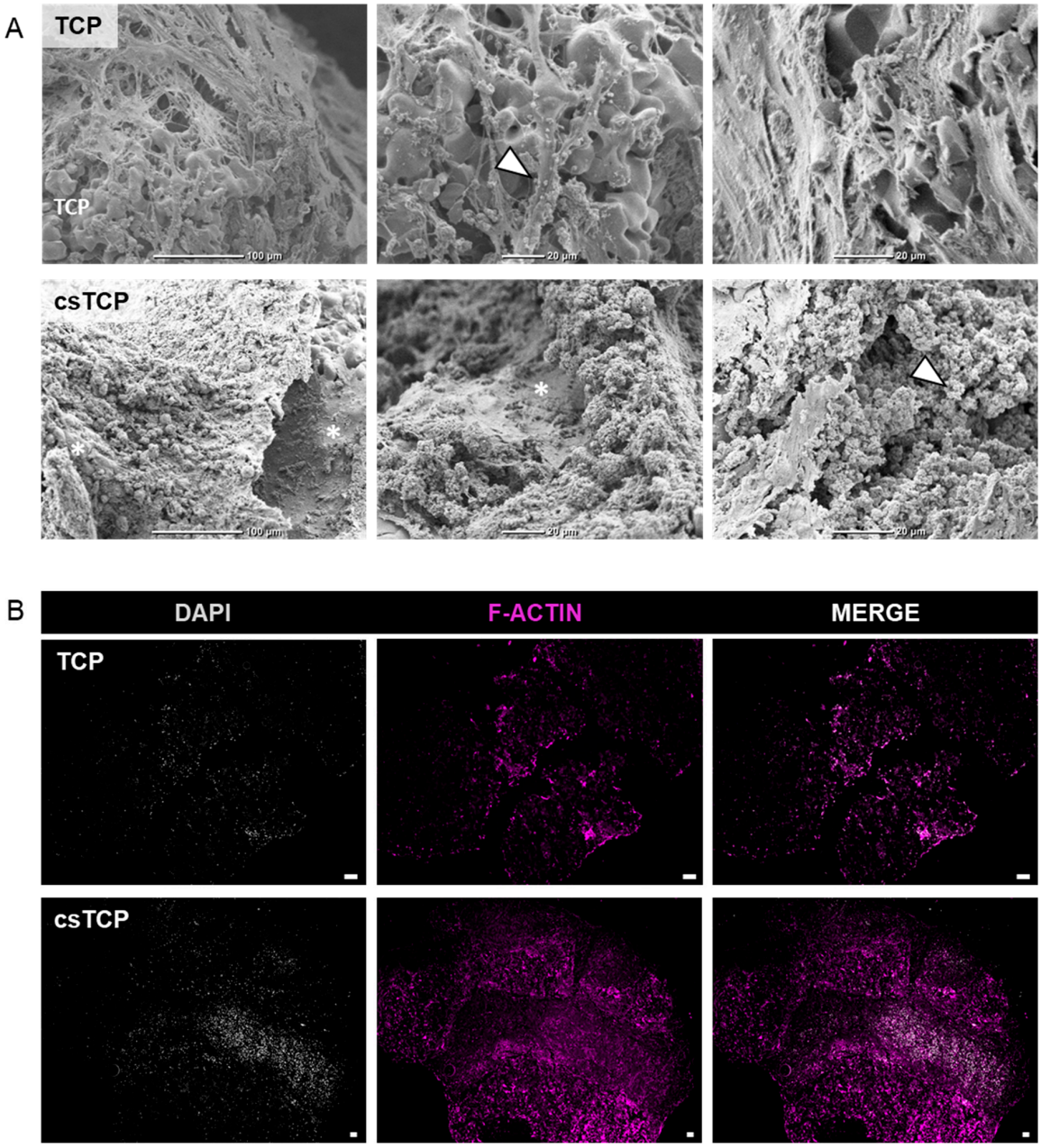

Figure 2. Comparing csTCPs and MSC-populated TCPs regarding cell density and morphology. (**A**) Exemplary SEM images at three magnifications highlighting cell adhesion, ECM content, phenotypic features at day 21 comparing TCP and csTCP. Cells well adhered to and spread on the surfaces of β-TCP. (**B**) Immunofluorescence staining for F-actin and DAPI to visualize cell density through the β-TCP particles. Exemplary images for n = 5. Scale bars show 100 µm. Legend: asterisk = highlighting ECM; arrow = highlighting microstructure deposition; TCP = highlighting the scaffold material.

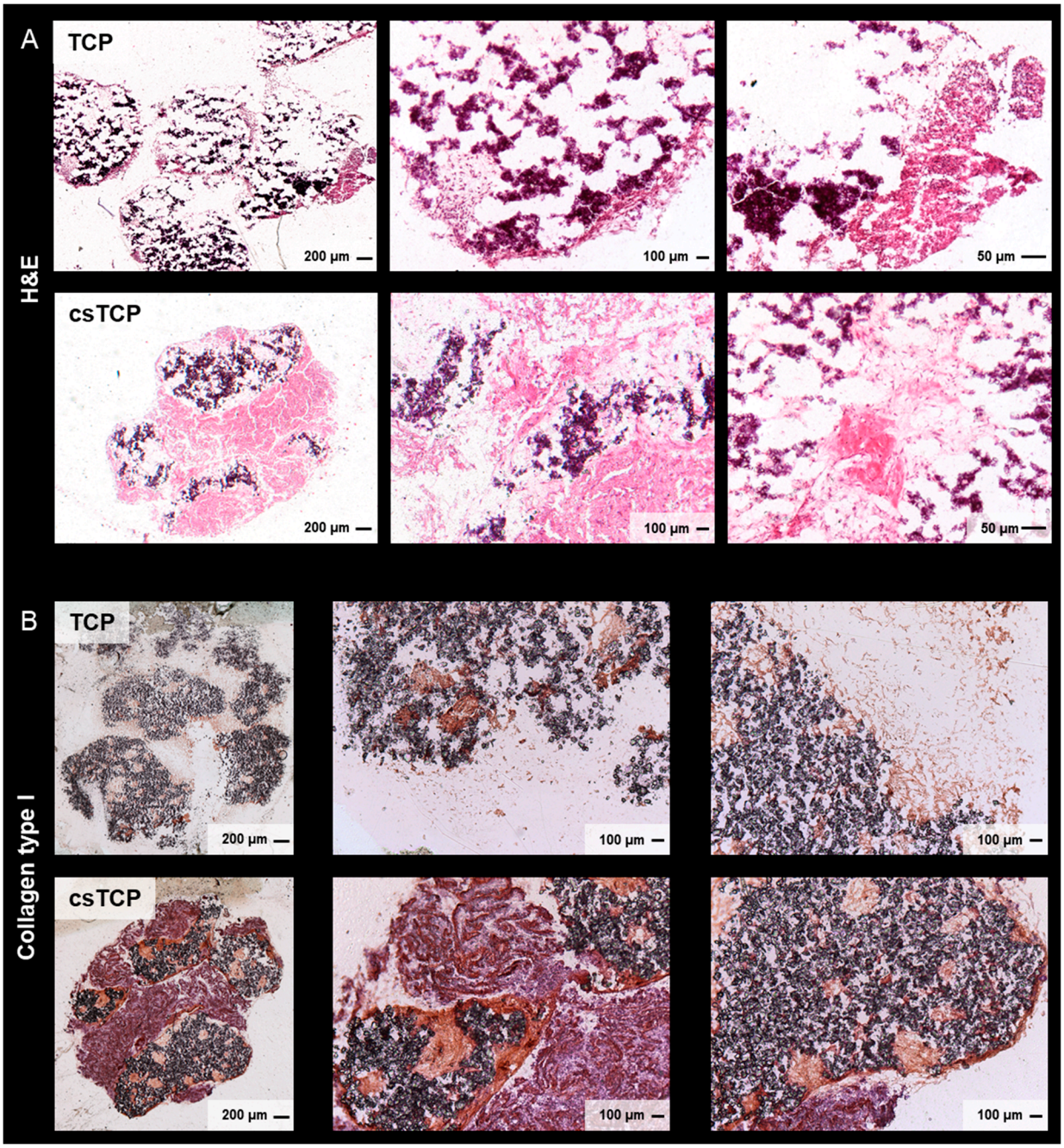

Figure 3. Comparing csTCPs and MSC-populated TCPs regarding uniform cell distribution and ECM at 21 days. (**A**) Representative images of hematoxylin and eosin (H & E) staining. (**B**) Exemplary images of histological sections stained for collagen type I and visualized using brightfield microscopy.

3.3. Sheet Technology Slightly Enhance Osteogenic Tissue Formation In Vitro

To analyze whether the combination of cell-sheet technology with β-TCP promotes osteogenic differentiation of MSCs, we monitored the relative mRNA expression levels of osteogenic marker genes, such as runt-related transcription factor 2 (*RUNX2*), osteopontin (*SPP1*), *COL1A1*, *OC*, alkaline phosphatase (*ALP*), and *ON* at 21 days using quantitative PCR. As a result, we observed a similar expression pattern of *RUNX2*—an early osteogenic marker—and *ALP* between TCP and csTCP. The expression of *SPP1*, *COL1A1*, and *ON* tended to be higher in csTCP, whereas the late-stage bone marker *OC* was significantly more highly expressed, compared to TCP.

In this line of observation, *PPARG* as an adipogenic marker gene and *SOX9* as a chondrogenic marker gene tended to be expressed less and significantly less, respectively, when TCP scaffolds were combined with sheet technology (Figure 4A). We further confirmed the *SPP1* gene expression result with immunofluorescence staining and noticed an intense staining of osteopontin at csTCP, as shown in Figure 4B. In summary, a clear osteogenic differentiation was achieved when using cell-sheet technology.

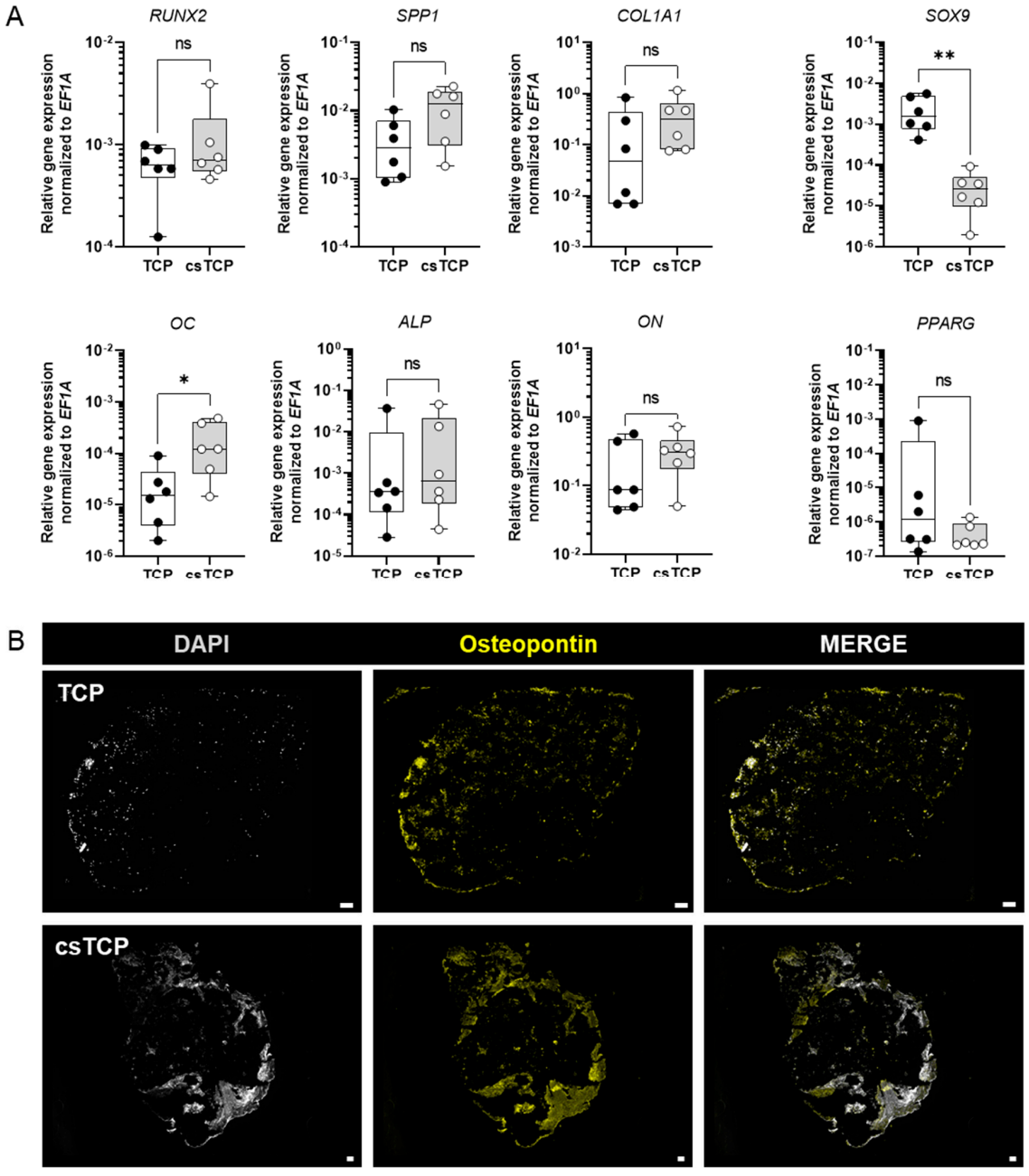

Figure 4. RNA expression analysis at day 21 showed that sheet technology slightly enhances osteogenic tissue formation in vitro. (**A**) Relative expression of osteogenic marker genes. Total RNA extraction was performed on day 21. Data are normalized to the housekeeper gene *EF1A*. Data are shown as box plots (centerline, median; box limits, upper and lower quartiles; whiskers, maximum and minimum values; all data points); $n = 6$. Statistics: Two-tailed Mann Whitney U test. *p*-values are indicated in the graphs with * $p < 0.05$, ** $p < 0.01$, ns = not significant. (**B**) Exemplary images of histological sections stained for osteopontin and visualized using a BZ-9000 fluorescence microscope ($n = 5$). Scale bars show 100 µm.

3.4. Deferoxamine Promotes Osteogenesis In Vitro

To confirm the responsiveness of our cell-sheet-based TCP bone model to modifying substances (e.g., therapeutics), we used DFO, which is well known to induce cellular hypoxia-adaptive, osteogenic, and angiogenic processes within the differentiated MSCs of the cell-sheet-based TCP bone model. Therefore, we treated csTCPs with 250 µM DFO for 3 days at day 21, compared them with the untreated control, and assessed the expression of selected marker genes. We observed an upregulation of osteogenic (*RUNX2*, *SPP1*), hypoxia-related (*LDHA*, *PGK1*, *VEGFA*), and pro-angiogenic (*VEGFA*, *IL8*) markers, while *IL6* was similarly expressed as compared to the untreated control (Figure 5). These experiments demonstrate the responsiveness of our cell-sheet-based TCP bone model to modifying substances, such as DFO.

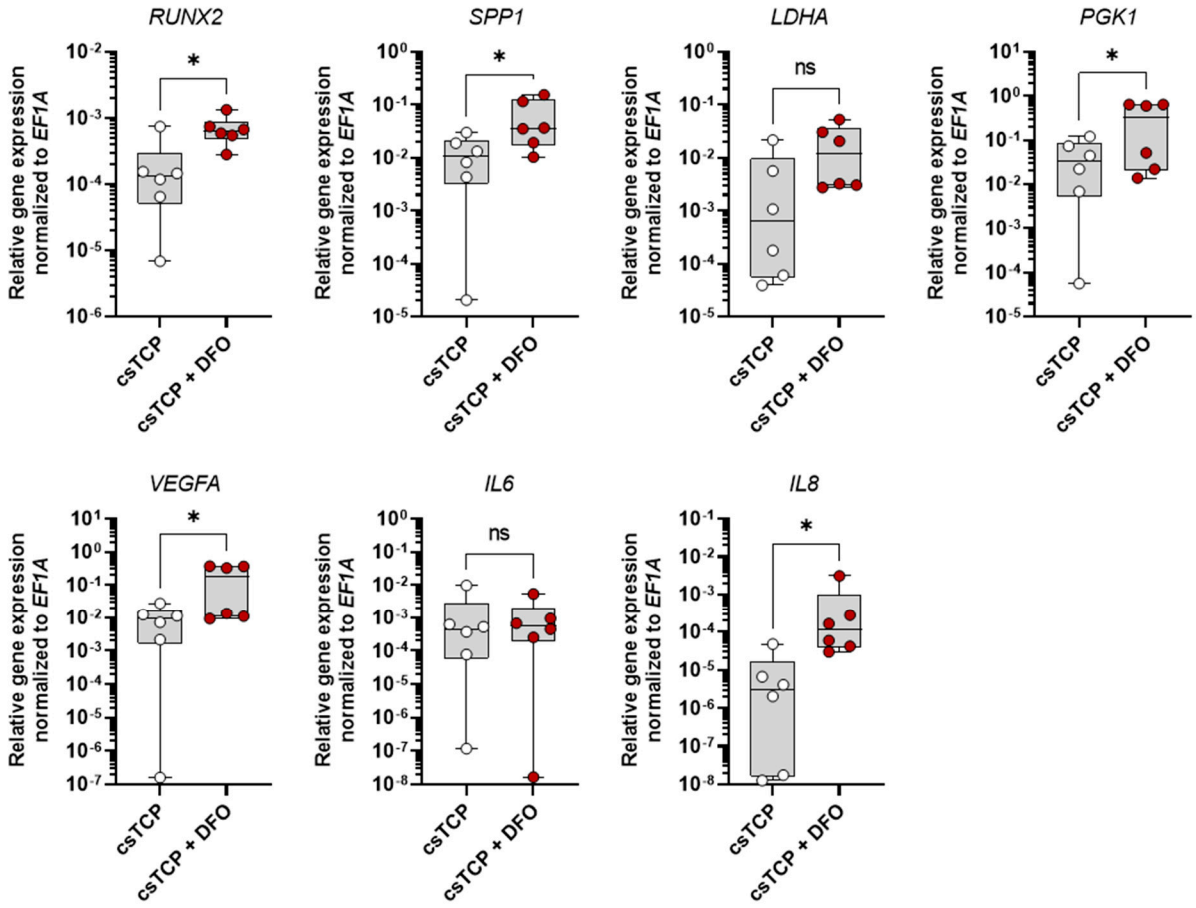

Figure 5. Deferoxamine (DFO) conditioned medium further promotes osteogenesis of the csTCP bone model verified on mRNA level using RT-qPCR. csTCP was treated after 21 days with 250 µM DFO for 72 h. Relative expression of *RUNX2*, *SPP1*, *LDHA*, *PGK1*, *VEGFA*, *IL6*, and *IL8* was normalized to the housekeeper gene *EF1A*. Data are shown as box plots (centerline, median; box limits, upper and lower quartiles; whiskers, maximum and minimum values; all data points); $n = 6$. Statistics: Two-tailed Wilcoxon matched-pairs signed-rank test. p-values are indicated in the graphs with * $p < 0.05$ and ns = not significant.

4. Discussion

In recent years, new advances have been made in bone tissue engineering to overcome the challenges of bone defect regeneration. Cell-sheet technology has become a promising tool, as its application to ectopic sites or bone defects promotes bone formation in vivo without using an additional scaffold [62,63]. Transplantation of mechanically generated osteogenic cell-sheets to the site of bone defects resulted in significantly improved new bone formation [64–66]. Fracture healing is characterized by initial inflammation, callus

formation, and bone remodeling, resulting in scar-free bone regeneration. In some cases, bone-healing disorders may occur, leading to delayed or non-union. Transplantation of osteogenic cell-sheets into a fractured rat femur showed improved bone formation at the fracture site, providing a treatment option for bone-healing disorders [67].

However, recapitulating the complex process of continuous bone remodeling in an adequate preclinical in vitro 3D model remains a significant challenge in the field of preclinical and basic musculoskeletal research [14]. Preclinical bone models as an alternative to the current gold standard—in vivo animal models—require the (co-)culture of bone-relevant cells under bone-like physiological conditions. Cell-sheets alone have poor mechanical properties and limited spatial support [16]. These obstacles can be surmounted by combining cell sheets with biodegradable scaffolds that mimic the mineral cancellous bone part.

The most common biodegradable scaffolds used as synthetic bone graft substitutes that closely resemble the native bone matrix are β-TCP, HA, and BCP (HA: β-TCP), well-known to be osteoconductive [68]. These materials facilitate cell adhesion, differentiation, and homogeneous cell distribution. The model or implant must be adjusted in particle size, pore size, porosity, and mechanical strength to the target natural bone, considering the different requirements of, for example, cortical and trabecular bone [60,69–71]. Macropores allow for cell proliferation due to the enhanced nutrient supply and oxygen transportation, while in vitro osteogenesis does not seem to be affected by pore size [72]. Trabecular bone has a porosity in the range of 50%–90% and a pore size up to 1000 µm in diameter [73].

In vitro bone models are used to mimic native cortical or trabecular bone to study physiological processes (e.g., metabolism of bone turnover), pathophysiological processes (e.g., cellular processes in bone healing), the effects of agents on bone homeostasis and regeneration (e.g., glucocorticoids or BMPs), implant integration (e.g., the interaction of bone and implant surfaces), or the suitability of the model as an implant itself (e.g., load-bearing capacity and stability) [2]. To evaluate substances or implant materials (evaluation of osteoconductive properties) in high-throughput format about toxicology, biocompatibility, tolerability, and osteoinductivity, simple, easy-to-handle scaffold-free spheroid cultures (osteospheres) with a 3D architecture but without mechanical strength are used [74–79]. In contrast, scaffold- or hydrogel-based models own load-bearing capacity and the option for a trabecular-like structure [80–87]. These models are more complex and bear the capability to add bone marrow cells, including immune cells, a supplying vascular-like system [86,87]. Typically scaffold-based models closely mimicking native bone are used to study physiological and pathophysiological processes and implant integration or serve as an implant itself. However, there is still space for optimization left.

The present study demonstrated that the biodegradable pre-seeded β-TCP scaffold or bone graft substitute wrapped with osteogenically induced MSC sheets exhibited higher expression of osteogenic genes and proteins in vitro. csTCP also showed sufficient matrix formation. Here, we evidenced that pre-seeded biodegradable β-TCP scaffolds wrapped with osteogenic MSC-sheets provide superior osteogenic performance in vitro and, therefore, may represent an elegant and physiologically relevant preclinical 3D alternative. Up-sizing of scaffold-based bone constructs becomes feasible through sheet technology. In addition, sheets combining different cell types can be fabricated, as demonstrated by Zhang et al. using MSC-derived endothelial progenitor cells on MSC sheets [88] and Kawamura et al. adding MSCs to human-induced pluripotent stem cell-derived cardiomyocyte sheets [89]. This provides the opportunity to combine osteoblast and osteoclast progenitor cells.

Artificial bone scaffold materials, such as TCP, are biodegradable and can be replaced by autologous bone after implantation. The β-TCP scaffold is one the most used and potent synthetic bone graft substitute known to be osteoconductive and osteoinductive [90,91]. The 3D structure with interconnected pores and an optimal porosity of 65% allows for sufficient nutrient supply, cell proliferation, and ingrowth of cells [92]. Ueha et al. demonstrated the promising osteogenic potential of pre-seeded TCP with osteogenic cell-sheets in a femoral defect model in rats [93]. A similar approach was applied to treat patients with osteoarthritis and/or osteonecrosis by using differentiated osteoblasts in combination with

scaffolds. Importantly, seeding cells on an artificial bone scaffold leads to bone formation, but only in their pores, resulting in single separated constructs without any bridging area. Considering the need for sophisticated preclinical in vitro 3D models, a physiologically similar bone with sufficient cell colonization and strong osteogenic potential should be developed to ensure the transferability of results. By confirming the cell adherence, cell phenotype, morphology, and cell density of differentiated MSCs on β-TCP with and without cell sheets, we successfully demonstrated an optimized cell seeding and the differentiation of MSCs using cell-sheet technology. Usually, the number of cells combined with artificial bone substitutes, such as β-TCP, is limited because most suspended cells remain in the pores and do not homogeneously and reproducibly populate the β-TCP scaffold as demonstrated here. Adding the cell sheet resulted in a large number of loaded cells on the β-TCP scaffold, thereby providing a microenvironment that facilitates cell seeding and differentiation. A strategy that optimizes seeding and production, up-sizing and osteogenic properties of small scale and small amounts of particles such as β-TCP particles. In this line of observation, Ueha et al. showed bone formation on the surface of sheet/TCP constructs, assuming facilitation in bridging the fracture gap and promoting bone formation [93]. Another sophisticated optimization approach of complex bone models in tissue engineering strategy is the functionalization of bioinspired scaffold systems. Functionalization with growth factors promoting angiogenesis and osteogenesis has shown great therapeutic potential in preclinical models and clinical applications [94,95]. They promote tissue ingrowth and proliferation. Growth factors such as VEGF, fibroblast growth factor (FGF) (involved in angiogenesis) as well as transforming growth factor-beta (TGF-β) and bone morphogenetic proteins (BMPs) (involved in healing and new bone formation) are commonly applied [96]. The latter is probably the most essential protein to enhance neo-bone formation in bone defects, such as tibia fracture reconstruction and spinal fusion surgery [97,98]. BMPs can be delivered to a surgical site by scaffold-based carrier systems, such as fibrous glass, HA granules, and β-TCP granules. Nowadays, these systems are chemically modified to enable the controlled, precise, sustained, and localized release of such proteins. Taken together, functionalized scaffolds allow mimicking hierarchical architectures and ECM components with high cell affinity and bioactivity, bringing the model closer to natural bone. In contrast, cell seeding and ingrowth can be optimized by enveloping them with an additional cell layer.

5. Conclusions

Our data demonstrate that the colonization of β-TCP scaffolds with MSCs and the additional wrapping of the colonized scaffolds creates a local niche. This niche promotes osteogenic but not chondrogenic and adipogenic differentiation and allows for the combination of multiple models. In addition, we have shown that our in vitro human MSC-sheet-based 3D bone model is responsive to modifying agents such as DFO. This finding suggests that optimization provides all the requirements to serve as an alternative personalized preclinical model of cancellous bone tissue for predicting and developing therapeutic strategies for treating bone healing disorders.

Although preclinical data from in vitro bone models and animal studies are often promising, the clinical failure of cell-based implants, osteoconductive bone substitutes, and osteoinductive growth factors cannot be predicted or generally excluded. Humans are complex systems that are more than the sum of their parts, which cannot be represented in all aspects by animal models or preclinical in vitro 3D models. Nevertheless, while animal models still remain models, preclinical in vitro 3D models can directly serve as bone graft substitutes for clinical application.

Author Contributions: Conceptualization, A.D. and T.G.; methodology, A.D.; validation, A.D.; formal analysis, A.D.; investigation, A.D.; data curation, A.D. and T.G.; writing—original draft preparation, A.D., T.G. and F.B.; writing—review and editing, A.D., T.G. and F.B.; visualization, A.D.; supervision, T.G.; project administration, F.B.; funding acquisition, T.G. and F.B. All authors have read and agreed to the published version of the manuscript.

Funding: This research was funded by the German Federal Ministry for Education and Research (BMBF), project number 031L0070A and Lush Prize Award 2018: Alexandra Damerau—Young Researcher, Rest of World. The work of A.D. was additionally supported by the German Academic Scholarship Foundation (Studienstiftung des deutschen Volkes) and by the Joachim Herz Foundation (Add-on Fellowship 2020). We acknowledge support from the German Research Foundation (DFG) and the Open Access Publication Fund of Charité-Universitätsmedizin Berlin.

Institutional Review Board Statement: The study was conducted in accordance with the Declaration of Helsinki, and approved by the Ethics Committee of the Charité-Universitätsmedizin Berlin (ethical approval EA1/012/13, January 2013; EA1/146/21, May 2021).

Informed Consent Statement: Informed consent was obtained from all subjects involved in the study.

Data Availability Statement: The data presented in this study are available on request from the corresponding author. The data are not publicly available due to privacy and ethical restrictions.

Acknowledgments: Bone marrow was provided by the Tissue Harvesting Core Facility of the BIH Berlin. A.D., F.B. and T.G. are members of the Berlin-Brandenburg research platform BB3R and Charité3R.

Conflicts of Interest: The authors declare no conflict of interest.

References

1. Alonzo, M.; Primo, F.A.; Kumar, S.A.; Mudloff, J.A.; Dominguez, E.; Fregoso, G.; Ortiz, N.; Weiss, W.M.; Joddar, B. Bone tissue engineering techniques, advances and scaffolds for treatment of bone defects. *Curr. Opin. Biomed. Eng.* **2021**, *17*, 100248. [CrossRef] [PubMed]
2. Pfeiffenberger, M.; Damerau, A.; Lang, A.; Buttgereit, F.; Hoff, P.; Gaber, T. Fracture Healing Research-Shift towards In Vitro Modeling? *Biomedicines* **2021**, *9*, 748. [CrossRef] [PubMed]
3. Einhorn, T.A.; Gerstenfeld, L.C. Fracture healing: Mechanisms and interventions. *Nat. Rev. Rheumatol* **2015**, *11*, 45–54. [CrossRef] [PubMed]
4. Collaborators, G.B.D.F. Global, regional, and national burden of bone fractures in 204 countries and territories, 1990–2019: A systematic analysis from the Global Burden of Disease Study 2019. *Lancet Healthy Longev.* **2021**, *2*, e580–e592. [CrossRef]
5. Salari, N.; Darvishi, N.; Bartina, Y.; Larti, M.; Kiaei, A.; Hemmati, M.; Shohaimi, S.; Mohammadi, M. Global prevalence of osteoporosis among the world older adults: A comprehensive systematic review and meta-analysis. *J. Orthop. Surg. Res.* **2021**, *16*, 669. [CrossRef]
6. Banaszkiewicz, P.A.; Kader, D.F. *Classic Papers in Orthopaedics*; Springer: London, UK, 2014; p. 624.
7. Zhu, G.; Zhang, T.; Chen, M.; Yao, K.; Huang, X.; Zhang, B.; Li, Y.; Liu, J.; Wang, Y.; Zhao, Z. Bone physiological microenvironment and healing mechanism: Basis for future bone-tissue engineering scaffolds. *Bioact. Mater.* **2021**, *6*, 4110–4140. [CrossRef] [PubMed]
8. Roddy, E.; DeBaun, M.R.; Daoud-Gray, A.; Yang, Y.P.; Gardner, M.J. Treatment of critical-sized bone defects: Clinical and tissue engineering perspectives. *Eur. J. Orthop. Surg. Traumatol.* **2018**, *28*, 351–362. [CrossRef]
9. Leenaars, C.H.C.; Kouwenaar, C.; Stafleu, F.R.; Bleich, A.; Ritskes-Hoitinga, M.; De Vries, R.B.M.; Meijboom, F.L.B. Animal to human translation: A systematic scoping review of reported concordance rates. *J. Transl. Med.* **2019**, *17*, 223. [CrossRef]
10. Bracken, M.B. Why animal studies are often poor predictors of human reactions to exposure. *J. R. Soc. Med.* **2009**, *102*, 120–122. [CrossRef]
11. Fong, E.L.S.; Toh, T.B.; Yu, H.; Chow, E.K. 3D Culture as a Clinically Relevant Model for Personalized Medicine. *SLAS Technol.* **2017**, *22*, 245–253. [CrossRef]
12. Mestas, J.; Hughes, C.C. Of mice and not men: Differences between mouse and human immunology. *J. Immunol.* **2004**, *172*, 2731–2738. [CrossRef] [PubMed]
13. Seok, J.; Warren, H.S.; Cuenca, A.G.; Mindrinos, M.N.; Baker, H.V.; Xu, W.; Richards, D.R.; McDonald-Smith, G.P.; Gao, H.; Hennessy, L.; et al. Genomic responses in mouse models poorly mimic human inflammatory diseases. *Proc. Natl. Acad. Sci. USA* **2013**, *110*, 3507–3512. [CrossRef] [PubMed]
14. Scheinpflug, J.; Pfeiffenberger, M.; Damerau, A.; Schwarz, F.; Textor, M.; Lang, A.; Schulze, F. Journey into Bone Models: A Review. *Genes* **2018**, *9*, 247. [CrossRef]
15. Roseti, L.; Parisi, V.; Petretta, M.; Cavallo, C.; Desando, G.; Bartolotti, I.; Grigolo, B. Scaffolds for Bone Tissue Engineering: State of the art and new perspectives. *Mater. Sci. Eng. C Mater. Biol. Appl.* **2017**, *78*, 1246–1262. [CrossRef] [PubMed]
16. Yorukoglu, A.C.; Kiter, A.E.; Akkaya, S.; Satiroglu-Tufan, N.L.; Tufan, A.C. A Concise Review on the Use of Mesenchymal Stem Cells in Cell Sheet-Based Tissue Engineering with Special Emphasis on Bone Tissue Regeneration. *Stem Cells Int.* **2017**, *2017*, 2374161. [CrossRef]
17. Owaki, T.; Shimizu, T.; Yamato, M.; Okano, T. Cell sheet engineering for regenerative medicine: Current challenges and strategies. *Biotechnol. J.* **2014**, *9*, 904–914. [CrossRef] [PubMed]

18. Murphy, M.B.; Suzuki, R.K.; Sand, T.T.; Chaput, C.D.; Gregory, C.A. Short Term Culture of Human Mesenchymal Stem Cells with Commercial Osteoconductive Carriers Provides Unique Insights into Biocompatibility. *J. Clin. Med.* **2013**, *2*, 49–66. [CrossRef]
19. Lomelino Rde, O.; Castro, S., II; Linhares, A.B.; Alves, G.G.; Santos, S.R.; Gameiro, V.S.; Rossi, A.M.; Granjeiro, J.M. The association of human primary bone cells with biphasic calcium phosphate (βTCP/HA 70:30) granules increases bone repair. *J. Mater. Sci. Mater. Med.* **2012**, *23*, 781–788. [CrossRef]
20. Bernhardt, A.; Lode, A.; Peters, F.; Gelinsky, M. Optimization of culture conditions for osteogenically-induced mesenchymal stem cells in β-tricalcium phosphate ceramics with large interconnected channels. *J. Tissue Eng. Regen. Med.* **2011**, *5*, 444–453. [CrossRef]
21. Shimizu, T.; Yamato, M.; Kikuchi, A.; Okano, T. Cell sheet engineering for myocardial tissue reconstruction. *Biomaterials* **2003**, *24*, 2309–2316. [CrossRef]
22. Yang, J.; Yamato, M.; Kohno, C.; Nishimoto, A.; Sekine, H.; Fukai, F.; Okano, T. Cell sheet engineering: Recreating tissues without biodegradable scaffolds. *Biomaterials* **2005**, *26*, 6415–6422. [CrossRef] [PubMed]
23. Takezawa, T.; Mori, Y.; Yoshizato, K. Cell culture on a thermo-responsive polymer surface. *Biotechnology* **1990**, *8*, 854–856. [CrossRef] [PubMed]
24. Li, M.; Ma, J.; Gao, Y.; Yang, L. Cell sheet technology: A promising strategy in regenerative medicine. *Cytotherapy* **2019**, *21*, 3–16. [CrossRef] [PubMed]
25. Moschouris, K.; Firoozi, N.; Kang, Y. The application of cell sheet engineering in the vascularization of tissue regeneration. *Regen. Med.* **2016**, *11*, 559–570. [CrossRef] [PubMed]
26. Ma, D.; Yao, H.; Tian, W.; Chen, F.; Liu, Y.; Mao, T.; Ren, L. Enhancing bone formation by transplantation of a scaffold-free tissue-engineered periosteum in a rabbit model. *Clin. Oral Implants Res.* **2011**, *22*, 1193–1199. [CrossRef] [PubMed]
27. Gao, Z.; Chen, F.; Zhang, J.; He, L.; Cheng, X.; Ma, Q.; Mao, T. Vitalisation of tubular coral scaffolds with cell sheets for regeneration of long bones: A preliminary study in nude mice. *Br. J. Oral Maxillofac. Surg.* **2009**, *47*, 116–122. [CrossRef] [PubMed]
28. Chen, F.; Zhou, Y.; Barnabas, S.T.; Woodruff, M.A.; Hutmacher, D.W. Engineering tubular bone constructs. *J. Biomech.* **2007**, *40* (Suppl. S1), S73–S79. [CrossRef]
29. Probst, F.A.; Fliefel, R.; Burian, E.; Probst, M.; Eddicks, M.; Cornelsen, M.; Riedl, C.; Seitz, H.; Aszodi, A.; Schieker, M.; et al. Bone regeneration of minipig mandibular defect by adipose derived mesenchymal stem cells seeded tri-calcium phosphate-poly(D,L-lactide-co-glycolide) scaffolds. *Sci. Rep.* **2020**, *10*, 2062. [CrossRef]
30. Ullah, I.; Subbarao, R.B.; Rho, G.J. Human mesenchymal stem cells—Current trends and future prospective. *Biosci. Rep.* **2015**, *35*, e00191. [CrossRef]
31. Bartholomew, A.; Sturgeon, C.; Siatskas, M.; Ferrer, K.; McIntosh, K.; Patil, S.; Hardy, W.; Devine, S.; Ucker, D.; Deans, R.; et al. Mesenchymal stem cells suppress lymphocyte proliferation in vitro and prolong skin graft survival in vivo. *Exp. Hematol.* **2002**, *30*, 42–48. [CrossRef]
32. Di Nicola, M.; Carlo-Stella, C.; Magni, M.; Milanesi, M.; Longoni, P.D.; Matteucci, P.; Grisanti, S.; Gianni, A.M. Human bone marrow stromal cells suppress T-lymphocyte proliferation induced by cellular or nonspecific mitogenic stimuli. *Blood* **2002**, *99*, 3838–3843. [CrossRef] [PubMed]
33. Stagg, J. Immune regulation by mesenchymal stem cells: Two sides to the coin. *Tissue Antigens* **2007**, *69*, 1–9. [CrossRef] [PubMed]
34. Ansari, S.; Ito, K.; Hofmann, S. Cell Sources for Human In vitro Bone Models. *Curr. Osteoporos. Rep.* **2021**, *19*, 88–100. [CrossRef] [PubMed]
35. Kang, Y.; Ren, L.; Yang, Y. Engineering vascularized bone grafts by integrating a biomimetic periosteum and β-TCP scaffold. *ACS Appl. Mater. Interfaces* **2014**, *6*, 9622–9633. [CrossRef] [PubMed]
36. Zhang, H.; Zhou, Y.; Zhang, W.; Wang, K.; Xu, L.; Ma, H.; Deng, Y. Construction of vascularized tissue-engineered bone with a double-cell sheet complex. *Acta Biomater.* **2018**, *77*, 212–227. [CrossRef] [PubMed]
37. Damerau, A.; Pfeiffenberger, M.; Weber, M.C.; Burmester, G.R.; Buttgereit, F.; Gaber, T.; Lang, A. A Human Osteochondral Tissue Model Mimicking Cytokine-Induced Key Features of Arthritis In Vitro. *Int. J. Mol. Sci* **2020**, *22*, 128. [CrossRef] [PubMed]
38. Wan, C.; Gilbert, S.R.; Wang, Y.; Cao, X.; Shen, X.; Ramaswamy, G.; Jacobsen, K.A.; Alaql, Z.S.; Eberhardt, A.W.; Gerstenfeld, L.C.; et al. Activation of the hypoxia-inducible factor-1α pathway accelerates bone regeneration. *Proc. Natl. Acad. Sci. USA* **2008**, *105*, 686–691. [CrossRef]
39. Donneys, A.; Ahsan, S.; Perosky, J.E.; Deshpande, S.S.; Tchanque-Fossuo, C.N.; Levi, B.; Kozloff, K.M.; Buchman, S.R. Deferoxamine restores callus size, mineralization, and mechanical strength in fracture healing after radiotherapy. *Plast. Reconstr. Surg.* **2013**, *131*, 711e–719e. [CrossRef]
40. Donneys, A.; Nelson, N.S.; Page, E.E.; Deshpande, S.S.; Felice, P.A.; Tchanque-Fossuo, C.N.; Spiegel, J.P.; Buchman, S.R. Targeting angiogenesis as a therapeutic means to reinforce osteocyte survival and prevent nonunions in the aftermath of radiotherapy. *Head Neck* **2015**, *37*, 1261–1267. [CrossRef]
41. Donneys, A.; Nelson, N.S.; Perosky, J.E.; Polyatskaya, Y.; Rodriguez, J.J.; Figueredo, C.; Vasseli, C.A.; Ratliff, H.C.; Deshpande, S.S.; Kozloff, K.M.; et al. Prevention of radiation-induced bone pathology through combined pharmacologic cytoprotection and angiogenic stimulation. *Bone* **2016**, *84*, 245–252. [CrossRef]
42. Donneys, A.; Weiss, D.M.; Deshpande, S.S.; Ahsan, S.; Tchanque-Fossuo, C.N.; Sarhaddi, D.; Levi, B.; Goldstein, S.A.; Buchman, S.R. Localized deferoxamine injection augments vascularity and improves bony union in pathologic fracture healing after radiotherapy. *Bone* **2013**, *52*, 318–325. [CrossRef] [PubMed]

43. Drager, J.; Ramirez-Garcia Luna, J.L.; Kumar, A.; Gbureck, U.; Harvey, E.J.; Barralet, J.E. Hypoxia Biomimicry to Enhance Monetite Bone Defect Repair. *Tissue Eng. Part A* **2017**, *23*, 1372–1381. [CrossRef] [PubMed]
44. Drager, J.; Sheikh, Z.; Zhang, Y.L.; Harvey, E.J.; Barralet, J.E. Local delivery of iron chelators reduces in vivo remodeling of a calcium phosphate bone graft substitute. *Acta Biomater.* **2016**, *42*, 411–419. [CrossRef] [PubMed]
45. Farberg, A.S.; Jing, X.L.; Monson, L.A.; Donneys, A.; Tchanque-Fossuo, C.N.; Deshpande, S.S.; Buchman, S.R. Deferoxamine reverses radiation induced hypovascularity during bone regeneration and repair in the murine mandible. *Bone* **2012**, *50*, 1184–1187. [CrossRef] [PubMed]
46. Guzey, S.; Aykan, A.; Ozturk, S.; Avsever, H.; Karslioglu, Y.; Ertan, A. The Effects of Desferroxamine on Bone and Bone Graft Healing in Critical-Size Bone Defects. *Ann. Plast. Surg.* **2016**, *77*, 560–568. [CrossRef] [PubMed]
47. Matsumoto, T.; Sato, S. Stimulating angiogenesis mitigates the unloading-induced reduction in osteogenesis in early-stage bone repair in rats. *Physiol. Rep.* **2015**, *3*, e12335. [CrossRef] [PubMed]
48. Shen, X.; Wan, C.; Ramaswamy, G.; Mavalli, M.; Wang, Y.; Duvall, C.L.; Deng, L.F.; Guldberg, R.E.; Eberhart, A.; Clemens, T.L.; et al. Prolyl hydroxylase inhibitors increase neoangiogenesis and callus formation following femur fracture in mice. *J. Orthop. Res. Off. Publ. Orthop. Res. Soc.* **2009**, *27*, 1298–1305. [CrossRef] [PubMed]
49. Stewart, R.; Goldstein, J.; Eberhardt, A.; Chu, G.T.; Gilbert, S. Increasing vascularity to improve healing of a segmental defect of the rat femur. *J. Orthop. Trauma* **2011**, *25*, 472–476. [CrossRef]
50. Yao, Q.; Liu, Y.; Tao, J.; Baumgarten, K.M.; Sun, H. Hypoxia-Mimicking Nanofibrous Scaffolds Promote Endogenous Bone Regeneration. *ACS Appl. Mater. Interfaces* **2016**, *8*, 32450–32459. [CrossRef] [PubMed]
51. Zhang, W.; Li, G.; Deng, R.; Deng, L.; Qiu, S. New bone formation in a true bone ceramic scaffold loaded with desferrioxamine in the treatment of segmental bone defect: A preliminary study. *J. Orthop. Sci. Off. J. Jpn. Orthop. Assoc.* **2012**, *17*, 289–298. [CrossRef]
52. Kang, H.; Yan, Y.; Jia, P.; Yang, K.; Guo, C.; Chen, H.; Qi, J.; Qian, N.; Xu, X.; Wang, F.; et al. Desferrioxamine reduces ultrahigh-molecular-weight polyethylene-induced osteolysis by restraining inflammatory osteoclastogenesis via heme oxygenase-1. *Cell Death Dis.* **2016**, *7*, e2435. [CrossRef] [PubMed]
53. Kusumbe, A.P.; Ramasamy, S.K.; Adams, R.H. Coupling of angiogenesis and osteogenesis by a specific vessel subtype in bone. *Nature* **2014**, *507*, 323–328. [CrossRef] [PubMed]
54. Li, J.; Fan, L.; Yu, Z.; Dang, X.; Wang, K. The effect of deferoxamine on angiogenesis and bone repair in steroid-induced osteonecrosis of rabbit femoral heads. *Exp. Biol. Med.* **2015**, *240*, 273–280. [CrossRef] [PubMed]
55. Liu, X.; Tu, Y.; Zhang, L.; Qi, J.; Ma, T.; Deng, L. Prolyl hydroxylase inhibitors protect from the bone loss in ovariectomy rats by increasing bone vascularity. *Cell Biochem. Biophys.* **2014**, *69*, 141–149. [CrossRef] [PubMed]
56. Wang, L.; Jia, P.; Shan, Y.; Hao, Y.; Wang, X.; Jiang, Y.; Yuan, Y.; Du, Q.; Zhang, H.; Yang, F.; et al. Synergistic protection of bone vasculature and bone mass by desferrioxamine in osteoporotic mice. *Mol. Med. Rep.* **2017**, *16*, 6642–6649. [CrossRef] [PubMed]
57. Donneys, A.; Yang, Q.; Forrest, M.L.; Nelson, N.S.; Zhang, T.; Ettinger, R.; Ranganathan, K.; Snider, A.; Deshpande, S.S.; Cohen, M.S.; et al. Implantable hyaluronic acid-deferoxamine conjugate prevents nonunions through stimulation of neovascularization. *NPJ Regen. Med.* **2019**, *4*, 11. [CrossRef] [PubMed]
58. Wagegg, M.; Gaber, T.; Lohanatha, F.L.; Hahne, M.; Strehl, C.; Fangradt, M.; Tran, C.L.; Schonbeck, K.; Hoff, P.; Ode, A.; et al. Hypoxia promotes osteogenesis but suppresses adipogenesis of human mesenchymal stromal cells in a hypoxia-inducible factor-1 dependent manner. *PLoS ONE* **2012**, *7*, e46483. [CrossRef] [PubMed]
59. Pfeiffenberger, M.; Damerau, A.; Ponomarev, I.; Bucher, C.H.; Chen, Y.; Barnewitz, D.; Thone-Reineke, C.; Hoff, P.; Buttgereit, F.; Gaber, T.; et al. Functional Scaffold-Free Bone Equivalents Induce Osteogenic and Angiogenic Processes in a Human In Vitro Fracture Hematoma Model. *J. Bone Miner. Res.* **2021**, *36*, 1189–1201. [CrossRef]
60. Stokovic, N.; Ivanjko, N.; Erjavec, I.; Milosevic, M.; Oppermann, H.; Shimp, L.; Sampath, K.T.; Vukicevic, S. Autologous bone graft substitute containing rhBMP6 within autologous blood coagulum and synthetic ceramics of different particle size determines the quantity and structural pattern of bone formed in a rat subcutaneous assay. *Bone* **2020**, *141*, 115654. [CrossRef] [PubMed]
61. Kazemzadeh-Narbat, M.; Kindrachuk, J.; Duan, K.; Jenssen, H.; Hancock, R.E.; Wang, R. Antimicrobial peptides on calcium phosphate-coated titanium for the prevention of implant-associated infections. *Biomaterials* **2010**, *31*, 9519–9526. [CrossRef]
62. Shimizu, K.; Ito, A.; Yoshida, T.; Yamada, Y.; Ueda, M.; Honda, H. Bone tissue engineering with human mesenchymal stem cell sheets constructed using magnetite nanoparticles and magnetic force. *J. Biomed. Mater. Res. B Appl. Biomater.* **2007**, *82*, 471–480. [CrossRef] [PubMed]
63. Ma, D.; Ren, L.; Liu, Y.; Chen, F.; Zhang, J.; Xue, Z.; Mao, T. Engineering scaffold-free bone tissue using bone marrow stromal cell sheets. *J. Orthop. Res.* **2010**, *28*, 697–702. [CrossRef] [PubMed]
64. Ueyama, Y.; Yagyuu, T.; Maeda, M.; Imada, M.; Akahane, M.; Kawate, K.; Tanaka, Y.; Kirita, T. Maxillofacial bone regeneration with osteogenic matrix cell sheets: An experimental study in rats. *Arch. Oral Biol.* **2016**, *72*, 138–145. [CrossRef] [PubMed]
65. Xie, Q.; Wang, Z.; Huang, Y.; Bi, X.; Zhou, H.; Lin, M.; Yu, Z.; Wang, Y.; Ni, N.; Sun, J.; et al. Characterization of human ethmoid sinus mucosa derived mesenchymal stem cells (hESMSCs) and the application of hESMSCs cell sheets in bone regeneration. *Biomaterials* **2015**, *66*, 67–82. [CrossRef]
66. Wang, F.; Hu, Y.; He, D.; Zhou, G.; Ellis, E., 3rd. Scaffold-free cartilage cell sheet combined with bone-phase BMSCs-scaffold regenerate osteochondral construct in mini-pig model. *Am. J. Transl. Res.* **2018**, *10*, 2997–3010.

67. Nakamura, A.; Akahane, M.; Shigematsu, H.; Tadokoro, M.; Morita, Y.; Ohgushi, H.; Dohi, Y.; Imamura, T.; Tanaka, Y. Cell sheet transplantation of cultured mesenchymal stem cells enhances bone formation in a rat nonunion model. *Bone* **2010**, *46*, 418–424. [CrossRef] [PubMed]
68. Zimmermann, G.; Moghaddam, A. Allograft bone matrix versus synthetic bone graft substitutes. *Injury* **2011**, *42* (Suppl. S2), S16–S21. [CrossRef]
69. Kasten, P.; Beyen, I.; Niemeyer, P.; Luginbuhl, R.; Bohner, M.; Richter, W. Porosity and pore size of β-tricalcium phosphate scaffold can influence protein production and osteogenic differentiation of human mesenchymal stem cells: An in vitro and in vivo study. *Acta Biomater.* **2008**, *4*, 1904–1915. [CrossRef]
70. Zhang, H.; Mao, X.; Du, Z.; Jiang, W.; Han, X.; Zhao, D.; Han, D.; Li, Q. Three dimensional printed macroporous polylactic acid/hydroxyapatite composite scaffolds for promoting bone formation in a critical-size rat calvarial defect model. *Sci. Technol. Adv. Mater.* **2016**, *17*, 136–148. [CrossRef]
71. Lee, D.J.; Kwon, J.; Kim, Y.I.; Wang, X.; Wu, T.J.; Lee, Y.T.; Kim, S.; Miguez, P.; Ko, C.C. Effect of pore size in bone regeneration using polydopamine-laced hydroxyapatite collagen calcium silicate scaffolds fabricated by 3D mould printing technology. *Orthod. Craniofac. Res.* **2019**, *22* (Suppl. S1), 127–133. [CrossRef]
72. Takahashi, Y.; Tabata, Y. Effect of the fiber diameter and porosity of non-woven PET fabrics on the osteogenic differentiation of mesenchymal stem cells. *J. Biomater. Sci. Polym. Ed.* **2004**, *15*, 41–57. [CrossRef] [PubMed]
73. Keaveny, T.M.; Morgan, E.F.; Niebur, G.L.; Yeh, O.C. Biomechanics of trabecular bone. *Annu. Rev. Biomed. Eng.* **2001**, *3*, 307–333. [CrossRef]
74. Kronemberger, G.S.; Matsui, R.A.M.; Miranda, G.d.A.S.d.C.E.; Granjeiro, J.M.; Baptista, L.S. Cartilage and bone tissue engineering using adipose stromal/stem cells spheroids as building blocks. *World J. Stem Cells* **2020**, *12*, 110–122. [CrossRef] [PubMed]
75. Shen, F.H.; Werner, B.C.; Liang, H.; Shang, H.; Yang, N.; Li, X.; Shimer, A.L.; Balian, G.; Katz, A.J. Implications of adipose-derived stromal cells in a 3D culture system for osteogenic differentiation: An in vitro and in vivo investigation. *Spine J.* **2013**, *13*, 32–43. [CrossRef]
76. Laschke, M.W.; Schank, T.E.; Scheuer, C.; Kleer, S.; Shadmanov, T.; Eglin, D.; Alini, M.; Menger, M.D. In vitro osteogenic differentiation of adipose-derived mesenchymal stem cell spheroids impairs their in vivo vascularization capacity inside implanted porous polyurethane scaffolds. *Acta Biomater.* **2014**, *10*, 4226–4235. [CrossRef] [PubMed]
77. Murata, D.; Tokunaga, S.; Tamura, T.; Kawaguchi, H.; Miyoshi, N.; Fujiki, M.; Nakayama, K.; Misumi, K. A preliminary study of osteochondral regeneration using a scaffold-free three-dimensional construct of porcine adipose tissue-derived mesenchymal stem cells. *J. Orthop. Surg. Res.* **2015**, *10*, 35. [CrossRef] [PubMed]
78. Fennema, E.M.; Tchang, L.A.H.; Yuan, H.; van Blitterswijk, C.A.; Martin, I.; Scherberich, A.; de Boer, J. Ectopic bone formation by aggregated mesenchymal stem cells from bone marrow and adipose tissue: A comparative study. *J. Tissue Eng. Regen. Med.* **2018**, *12*, e150–e158. [CrossRef]
79. Brochado, A.C.B.; de Souza, V.H.; Correa, J.; Dos Anjos, S.A.; de Almeida Barros Mourao, C.F.; Cardarelli, A.; Montemezzi, P.; Gameiro, V.S.; Pereira, M.R.; Mavropoulos, E.; et al. Osteosphere Model to Evaluate Cell-Surface Interactions of Implantable Biomaterials. *Materials* **2021**, *14*, 5858. [CrossRef]
80. Ishaug-Riley, S.L.; Crane, G.M.; Gurlek, A.; Miller, M.J.; Yasko, A.W.; Yaszemski, M.J.; Mikos, A.G. Ectopic bone formation by marrow stromal osteoblast transplantation using poly(DL-lactic-co-glycolic acid) foams implanted into the rat mesentery. *J. Biomed. Mater. Res.* **1997**, *36*, 1–8. [CrossRef]
81. Chen, L.J.; Wang, M. Production and evaluation of biodegradable composites based on PHB-PHV copolymer. *Biomaterials* **2002**, *23*, 2631–2639. [CrossRef]
82. Yaszemski, M.J.; Payne, R.G.; Hayes, W.C.; Langer, R.; Mikos, A.G. Evolution of bone transplantation: Molecular, cellular and tissue strategies to engineer human bone. *Biomaterials* **1996**, *17*, 175–185. [CrossRef]
83. Hu, Y.; Grainger, D.W.; Winn, S.R.; Hollinger, J.O. Fabrication of poly(α-hydroxy acid) foam scaffolds using multiple solvent systems. *J. Biomed. Mater. Res.* **2002**, *59*, 563–572. [CrossRef] [PubMed]
84. Sheikh, F.A.; Ju, H.W.; Moon, B.M.; Lee, O.J.; Kim, J.-H.; Park, H.J.; Kim, D.W.; Kim, D.-K.; Jang, J.E.; Khang, G.; et al. Hybrid scaffolds based on PLGA and silk for bone tissue engineering. *J. Tissue Eng. Regen. Med.* **2016**, *10*, 209–221. [CrossRef] [PubMed]
85. Yao, Q.; Cosme, J.G.; Xu, T.; Miszuk, J.M.; Picciani, P.H.; Fong, H.; Sun, H. Three dimensional electrospun PCL/PLA blend nanofibrous scaffolds with significantly improved stem cells osteogenic differentiation and cranial bone formation. *Biomaterials* **2017**, *115*, 115–127. [CrossRef] [PubMed]
86. Bose, S.; Tarafder, S. Calcium phosphate ceramic systems in growth factor and drug delivery for bone tissue engineering: A review. *Acta Biomater.* **2012**, *8*, 1401–1421. [CrossRef] [PubMed]
87. Matsuno, T.; Hashimoto, Y.; Adachi, S.; Omata, K.; Yoshitaka, Y.; Ozeki, Y.; Umezu, Y.; Tabata, Y.; Nakamura, M.; Satoh, T. Preparation of injectable 3D-formed β-tricalcium phosphate bead/alginate composite for bone tissue engineering. *Dent. Mater. J.* **2008**, *27*, 827–834. [CrossRef] [PubMed]
88. Zhang, R.; Gao, Z.; Geng, W.; Yan, X.; Chen, F.; Liu, Y. Engineering vascularized bone graft with osteogenic and angiogenic lineage differentiated bone marrow mesenchymal stem cells. *Artif. Organs* **2012**, *36*, 1036–1046. [CrossRef]
89. Kawamura, M.; Miyagawa, S.; Fukushima, S.; Saito, A.; Miki, K.; Funakoshi, S.; Yoshida, Y.; Yamanaka, S.; Shimizu, T.; Okano, T.; et al. Enhanced Therapeutic Effects of Human iPS Cell Derived-Cardiomyocyte by Combined Cell-Sheets with Omental Flap Technique in Porcine Ischemic Cardiomyopathy Model. *Sci. Rep.* **2017**, *7*, 8824. [CrossRef]

90. Bohner, M.; Santoni, B.L.G.; Dobelin, N. Beta-Tricalcium phosphate for bone substitution: Synthesis and properties. *Acta Biomater.* **2020**, *113*, 23–41. [CrossRef]
91. Liu, G.; Zhao, L.; Cui, L.; Liu, W.; Cao, Y. Tissue-Engineered bone formation using human bone marrow stromal cells and novel beta-tricalcium phosphate. *Biomed. Mater.* **2007**, *2*, 78–86. [CrossRef]
92. Gao, P.; Zhang, H.; Liu, Y.; Fan, B.; Li, X.; Xiao, X.; Lan, P.; Li, M.; Geng, L.; Liu, D.; et al. Beta-Tricalcium phosphate granules improve osteogenesis in vitro and establish innovative osteo-regenerators for bone tissue engineering in vivo. *Sci. Rep.* **2016**, *6*, 23367. [CrossRef] [PubMed]
93. Ueha, T.; Akahane, M.; Shimizu, T.; Uchihara, Y.; Morita, Y.; Nitta, N.; Kido, A.; Inagaki, Y.; Kawate, K.; Tanaka, Y. Utility of tricalcium phosphate and osteogenic matrix cell sheet constructs for bone defect reconstruction. *World J. Stem Cells* **2015**, *7*, 873–882. [CrossRef] [PubMed]
94. Wang, Z.; Wang, K.; Lu, X.; Li, M.; Liu, H.; Xie, C.; Meng, F.; Jiang, O.; Li, C.; Zhi, W. BMP-2 encapsulated polysaccharide nanoparticle modified biphasic calcium phosphate scaffolds for bone tissue regeneration. *J. Biomed. Mater. Res. A* **2015**, *103*, 1520–1532. [CrossRef]
95. Zhang, H.; Migneco, F.; Lin, C.Y.; Hollister, S.J. Chemically-Conjugated bone morphogenetic protein-2 on three-dimensional polycaprolactone scaffolds stimulates osteogenic activity in bone marrow stromal cells. *Tissue Eng. Part A* **2010**, *16*, 3441–3448. [CrossRef] [PubMed]
96. Blumenfeld, I.; Srouji, S.; Lanir, Y.; Laufer, D.; Livne, E. Enhancement of bone defect healing in old rats by TGF-beta and IGF-1. *Exp. Gerontol.* **2002**, *37*, 553–565. [CrossRef]
97. Seeherman, H.; Wozney, J.M. Delivery of bone morphogenetic proteins for orthopedic tissue regeneration. *Cytokine Growth Factor Rev.* **2005**, *16*, 329–345. [CrossRef] [PubMed]
98. Dimar, J.R.; Glassman, S.D.; Burkus, K.J.; Carreon, L.Y. Clinical outcomes and fusion success at 2 years of single-level instrumented posterolateral fusions with recombinant human bone morphogenetic protein-2/compression resistant matrix versus iliac crest bone graft. *Spine* **2006**, *31*, 2534–2539; discussion 2540. [CrossRef]